Opto-Electronic Advances

ISSN 2096-4579 CN 51-1781/TN

An externally perceivable smart leaky-wave antenna based on spoof surface plasmon polaritons

Weihan Li, Jia Chen, Shizhao Gao, Lingyun Niu, Jiaxuan Wei, Ruosong Sun, Yaqi Wei, Wenxuan Tang and Tie Jun Cui

Citation: Li WH, Chen J, Gao SZ, et al. An externally perceivable smart leaky-wave antenna based on spoof surface plasmon polaritons. *Opto-Electron Adv* **7**, 240040(2024).

https://doi.org/10.29026/oea.2024.240040

Received: 11 April 2024; Accepted: 17 June 2024; Published online: 9 August 2024

Opto-Electronic Advances

Article

September 2024, Vol. 7, No. 9

DOI: 10.29026/oea.2024.240040

An externally perceivable smart leaky-wave antenna based on spoof surface plasmon polaritons

Weihan Li[1,2], Jia Chen[1,2], Shizhao Gao[1,2], Lingyun Niu[1,2], Jiaxuan Wei[1,2], Ruosong Sun[1,2], Yaqi Wei[1,2], Wenxuan Tang[1,2]* and Tie Jun Cui[1,2]*

Smart antennas have received great attention for their potentials to enable communication and perception functions at the same time. However, realizing the function synthesis remains an open challenge, and most existing system solutions are limited to narrow operating bands and high complexity and cost. Here, we propose an externally perceivable leaky-wave antenna (LWA) based on spoof surface plasmon polaritons (SSPPs), which can realize adaptive real-time switching between the “radiating” and “non-radiating” states and beam tracking at different frequencies. With the assistance of computer vision, the smart SSPP-LWA is able to detect the external target user or jammer, and intelligently track the target by self-adjusting the operating frequency. The proposed scheme helps to reduce the power consumption through dynamically controlling the radiating state of the antenna, and improve spectrum utilization and avoid spectrum conflicts through intelligently deciding the radiating frequency. On the other hand, it is also helpful for the physical layer communication security through switching the antenna working state according to the presence of the target and target beam tracking in real time. In addition, the proposed smart antenna can be generalized to other metamaterial systems and could be a candidate for synaesthesia integration in future smart antenna systems.

Keywords: smart antenna; external perception; spoof surface plasmon polaritons; computer vision aids

Li WH, Chen J, Gao SZ et al. An externally perceivable smart leaky-wave antenna based on spoof surface plasmon polaritons. *Opto-Electron Adv* **7**, 240040 (2024).

Introduction

In the era of fifth-generation (5G) wireless communications where devices are heavily used, due to the great advances in the Internet of Things (IoT) and artificial intelligence (AI), perceivable devices with miniaturization and flexible regulations are facilitated for managing the wireless channels, and many interesting applications are therefore developed. Hence, in the physical level, the wireless channel and electromagnetic (EM) link between the transmitter and receiver with complex propagation internally play an important role in the future wireless communications.

On the other hand, surface plasmon polariton (SPP) in the optical frequency region[1] is a special kind of surface wave restricted to the interface between two media with opposite signs of permittivity. In order to realize spoof SPPs (SSPPs) in the terahertz and microwave bands, many efforts have been made[2,3]. In particular, SSPPs transmission lines (TLs) with ultrathin substrate and metallic structures have been presented and attracted

[1]State Key Laboratory of Millimeter Waves, Southeast University, Nanjing 210096, China; [2]Institute of Electromagnetic Space, Southeast University, Nanjing 210096, China.

*Correspondence: WX Tang, Email: wenxuant@seu.edu.cn; TJ Cui, Email: tjcui@seu.edu.cn

Received: 11 April 2024; Accepted: 17 June 2024; Published online: 9 August 2024

many interests[4,5]. In recent years, lots of planar SSPPs devices have been proposed, such as low-loss transmission lines[6,7], filters[8,9], couplers[10,11], amplifier[12,13], backward phase matching[14] and others[15–17]. The planar SSPPs have the characteristics of outstanding field-confinement, flexible dispersion regulation, low pass nature, wide band, low cost, and lightweight and compact properties, and therefore have great potentials in future wireless communication systems. Furthermore, some ultra-thin spoof metasurface, due to their modulation of the dispersion of structured light on the subwavelength scale, give rise to beam deflector[18] and integrated imaging[19,20].

Specifically, many excellent characteristics of SSPP electromagnetic materials such as flexible design, greater slow-wave, EM coupling, low cost, low loss, low profile, etc., make it more conducive to the design of antennas, which can control the near field by the control unit arrangement to change the radiation effect in the far field. For example, as one type of beam-scanning antennas (BSA), leaky-wave antennas (LWA) with periodic radiation elements or continuous apertures[21,22] are widely used in radar and wireless communication systems for their low profile and easy integration into the surface of carriers[23–26]. Compared with the conventional feeding structures, the LWA based on the SSPP structure has the characteristics of simple and flexible design, more flexible bandwidth design, and more consistent gain in the frequency band, which can achieve the advantages of large scanning angle, wide working band and high gain[27,28]. At present, Most of the SSPP-LWAs could be divided into two types according to the radiation schemes: periodic modulation and EM coupling. For the first type, SSPP-LWA is modulated periodically in the waveguide structure to excite an infinite number of space harmonics and thus radiate[29,30]. In contrast, the SSPP antennas based on EM coupling[31–33] are generally in the form of periodic radiation cells located close to the SSPP TL for energy coupling and radiation. Compared to the first type, the independent design of the feed SSPP TL and the radiation units greatly improves the degree of freedom of design, and can be designed with shorter antenna lengths to achieve higher gain.

Hence, the reconfigurable SSPP-LWA is very suitable for developing a new type of smart antenna because of the outstanding ability of dispersion regulation and high freedom of wave control. The field of smart antenna is constantly evolving, generally including the following three categories. First, beamforming antennas[34–37] focus the signal by dynamically adjusting the antennas' orientation, providing more powerful signal coverage and quality. However, complex hardware and signal processing requirements are required, which increases the system cost. Also, adaptability to dynamic environments may present some challenges. The second category, adaptive antennas[38,39], adjusts antenna parameters in real time to improve signal quality and combat signal interference, but the hardware and algorithms are more complex and require a lot of computing resources to support. The third one, multi-functional metasurfaces[40–43] and reconfigurable intelligence surfaces[44–47]. The former achieves full-space functions by flexibly adjusting the phase or polarization of the unit, enabling capabilities like transmission-reflection-integrated[40,43], tunable holograms[42], and optical sensing[41]. The latter is to optimize signal channels by adjusting surface reflection properties, and have great potentials to improve signal coverage and capacity. However, complex control and communication systems are usually required in this case. Recently, metasurfaces and sensors have been combined to enable a lot of work in intelligent EM control system[48–51]. For example, metasurfaces combined with computer vision (CV) relies on cameras, data and algorithms to receive instructions or take actions such as beam tracking[52,53], remote sensing image[54], traffic surveillance system[55,56]. Among them, intelligent metasurface systems[53] based on CV have been developed for EM tracking and real-time wireless communication of moving targets. EM characteristics of each unit cell in the metasurface is electrically tuned for the realization of real-time beams forming with high accuracy and flexibility. However, due to limitations in manufacturing complexity and power consumption, there exist some technical challenges in the intelligent metasurface systems. In view of the above, SSPP-LWA with self-reconfigurable operating frequency and auto switch of radiation state is especially required in spectrum analysis and wide-band communication applications. The SSPP antenna possess much less unit cells than the metasurface, and therefore is relatively simple to manufacture and easy to modulate.

In this paper, we propose a new approach combining reconfigurable SSPP-LWA with CV as a smart antenna system to realize the global management of wireless channels in the process of transmission, and automatically meet the needs of users in dynamic environment. By adding PIN diodes on the radiating element and adjusting the bias voltage of the PIN diode, the working

state (e.g., the radiating state and the non-radiating state) is controlled dynamically within the frequency band. Experiments show that in the "radiating" state, the beam scanning range of the reconfigurable SSPP-LWA is −43°~5° in the frequency band from 8.5 to 13 GHz. Next, visual information is employed to assist SSPP-LWA in adjusting beam scanning. The proposed vision-based scheme utilizes advanced CV technology to acquire the position information of the user relative to the reconfigurable SSPP-LWA, sends the position information to the computer, and then feedbacks instructions to the FPGA and signal generator. We provide two experiment scenarios. In the first one, the camera is used to detect whether there is a target in the specified range, and the adaptive real-time switching between the radiation state and the non-radiation state is realized accordingly. In the second scenario, the SSPP-LWA provides feedback on the base station side according to the target position, and supplies the desired frequency instruction in line with the direction towards the selected target, thereby realizing beam tracking.

The proposed reconfigurable SSPP-LWA combined with CV can perceive the moving targets through target detection, and then dynamically adjust the use of spectrum resources. In wide-band communication, the SSPP-LWA can adjust the operating frequency according to this information to avoid spectrum conflict and improve spectrum utilization. In the optimization of energy efficiency, combined with the real-time perception of CV, the smart SSPP-LWA can more intelligently select the operating mode and frequency in wide-band communication to optimize the energy efficiency of the communication system, reduce power consumption. Also, the smart SSPP-LWA can switch the antenna working state according to the presence of the target and realize target beam tracking in real time, enhance physical layer communication security.

Results and discussion

Architecture of the intelligent scheme

The schematic of the proposed intelligent system is presented in Figs. 1 and 2, which is composed of the reconfigurable SSPP-LWA and an RGB-Depth camera. The moving target is represented by a model car or the target user (e.g., here a broadband horn antenna is used as the target user for signal reception) moving along a certain path. The images of the car (or the broadband horn antenna) are taken by an Intel RealSense Depth Camera D435i (RS-Camera) located on the SSPP-LWA at the rate of 40 FPS (frames per second), and each image is selected by the convolutional neural network (CNN) based on YOLOv4-tiny. The original image is firstly scaled to [608, 608, 3] when reasoning, and then input to the CSPDarknet53-tiny network for the feature extraction. After passing through five groups of convolution and pooling layers, the feature maps with three different dimensions are obtained, which are fused by the network and YOLO layers. We optimize the network to not only detect the target, but also collect its position and its elevation and azimuth angles in the coordinates of the RS-Camera.

The moving object is tracked dynamically and its position information is refreshed in real-time by the RS-Camera, with each refresh followed by a voltage control sequence that feeds the FPGA or by the corresponding frequency signal that feeds the signal generator connected to the reconfigurable SSPP-LWA. The input voltage and frequency of the reconfigurable SSPP-LWA is obtained through the computer using the feedback information, and the instruction are constantly refreshed. In the first experimental scenario, by the voltage that feedback from detecting whether there are external objects within a specific range, the smart SSPPs LWA can realize the adaptive real-time switching between the radiation state and the non-radiation state. In the second experimental scenario, the smart SSPP-LWA is carefully designed to transmit a frequency-dependent scanning beam towards the moving target with regard to its changing positions. Among them, the coordinate systems of the camera and the reconfigurable SSPP-LWA (as they are closely located) are unified to ensure the accuracy of the position.

Functional demonstrations of the reconfigurable SSPP-LWA

Theory of radiation

The theoretical analysis in this section includes two parts, one is reconfiguration of state switching in the operating frequency band, and the other is frequency-controlled beam scanning of the SSPP-LWA when PIN diode is turned on.

Firstly, the radiation principle of the SSPP-LWA is analyzed. The dispersion curve of SSPPs TL is taken as the starting point, as shown in Fig. 3. It can be seen that the dispersion curve for the fundamental mode of SSPPs TL

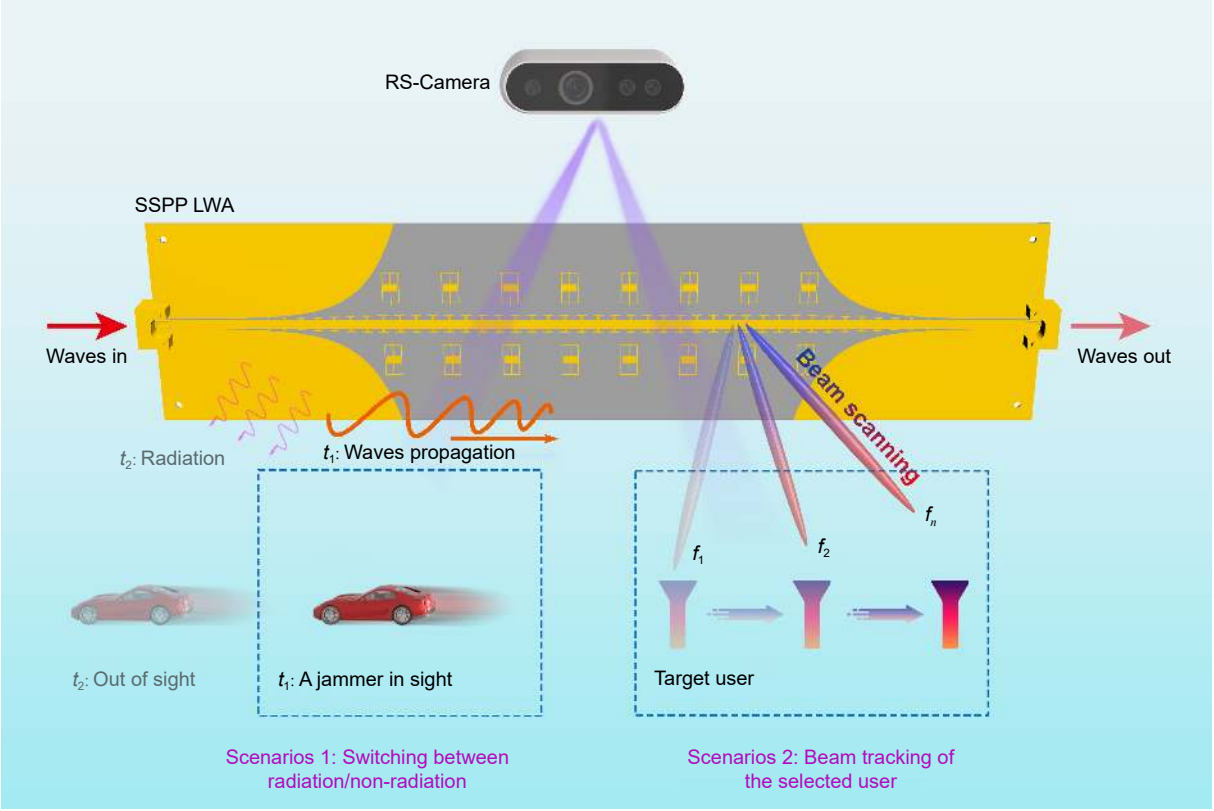

Fig. 1 | Schematic of the smart SSPP-LWA system. The RS-camera automatically detects the moving target - a model car or a target user (e.g., a horn here) in the environment. The position information of the target is sent to the control system, the supply voltage (via a FPGA) or input frequency (via a signal generator) is fed back in a few milliseconds, and the working status of SSPP-LWA is altered or the beam tracking are realized.

(the red curve with n=0) is located on the right side of the light line, that is, SSPPs present a slow-wave property and cannot be radiated directly. Radiation of EM waves to free space requires two steps: the first step is coupling from the SSPPs TL to the radiation patch, and the second step is radiating through the patch unit into free space. Theoretical calculations of the radiation pattern are given in Supplementary information Section 1 for details. According to the Floquet theory analysis, periodic placement of radiation unit cells near SSPPs TLs can excite an infinite number of spatial harmonics:

$$k_n = k_{\rm spp} + \frac{2n\pi}{d}, n = 0, \pm1, \pm2 \cdots \quad (1)$$

where $k_{\rm spp}$ is the propagation constant of the n = 0 harmonic (the fundamental mode), and d is the distance between two adjacent radiation unit cells. In Fig. 3, n represents the n-th harmonic. Partly harmonics with n=−1 and n=−2 are located within the fast wave region of the optical cone and can be radiated. To be noted, if n≤−2 space harmonics are designed to radiate fast waves, then −1 spatial harmonics can also radiate[57]. In order to obtain pure mode radiation, in practice −1-th harmonic is usually selected for radiation. Here the radiation frequency band is between the frequency points of A and B in Fig. 3. According to Eq. (1), it is found that the radiation frequency band is closely related to the distance between the two radiation unit cells, and hence one can calculate the distance d between the two radiation unit cells according to the required working frequency band. A specific frequency point f_0 is designed as the normal radiant point, at this time k_{-1} is 0, so $d = 2\pi/(k_{\rm spp}|f_0)$, where $(k_{\rm spp}|f_0)$ represents the propagation constant of the fundamental wave at the specific frequency f_0, it can be see that the period between the radiation unit is consistent with the wavelength of the SSPPs at the specific frequency f_0, And we can obtain $(k_{\rm spp}|f_0)$ through Fig. 3, thus the distance between two radiation unit cells can be designed.

The detailed structure of reconfigurable SSPP-LWA is shown in Fig. 4. An SSPPs TL with miniaturization, strong field binding and high EM energy density is expected. Therefore, an SSPPs TL with "T"-shaped units was designed through modifying the unit's height. The rectangular structures on both sides of the commonly

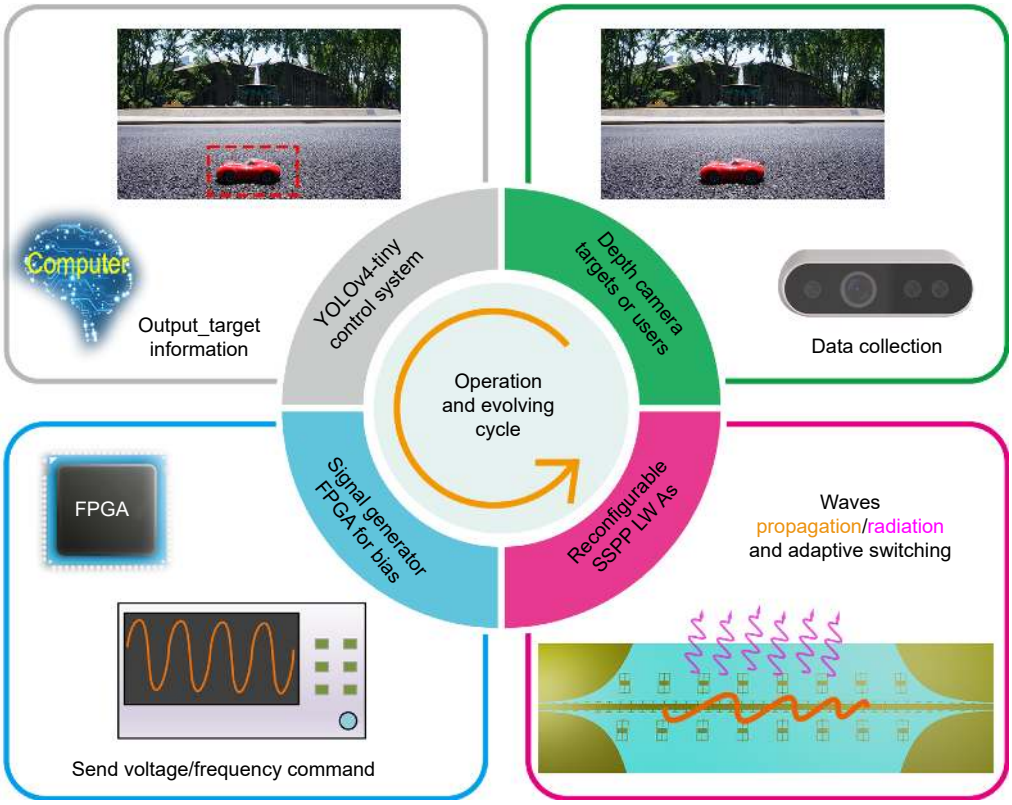

Fig. 2 | Smart SSPP-LWA operation architecture. There are four main components in the operation cycle. The depth camera is used for capturing picture information. Through the control system based on YOLOv4-tiny pre-training module, the target detection task is completed. Two devices, the FPGA and the signal generator, are used to control the voltage and input frequency signal to control the reconfigurable SSPP-LWA. Finally, the smart SSPP-LWA can realize the adaptive real-time switching between the radiation and the non-radiation of EM waves and beam tracking.

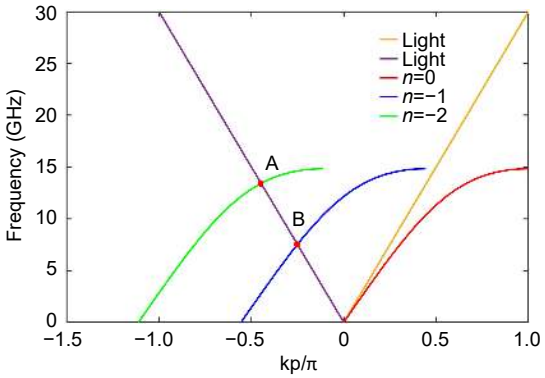

Fig. 3 | Dispersion curves of space harmonics.

used H-shaped SSPP units were bent to both sides respectively, and the "T"-shaped unit structure was finally determined, as shown in Fig. 4(c). For validations, an SSPPs TL is fabricated, and its performance has been verified, maintaining a higher transmission coefficient and lower reflection coefficient. Please see Supplementary information Section 2 for details.

The switchable radiating/non-radiating working state is caused by the change of the state of the PIN diodes embedded in the radiating patch, which are mounted on either side of the ELC resonant structure, as shown in Fig. 4(c). The topological circuit of the PIN diode, that is, how to position the PIN diode, is critical for the working bandwidth and gain isolation of the two working states. In addition, as shown in Fig. 4(d), the structure of the middle capacitor is thicker than usual, which helps to optimize the influence between the two operating states. For simulated transmission coefficient of the reconfigurable SSPP-LWA with different number of diodes, please see Supplementary information Section 3 for details. The PIN diodes are embedded in the approximate middle of both sides of the radiating element and are connected in series, in which the distance *pd* between the two diodes is 1.1 mm. In addition, the via hole on the radiation patch close to the TL are connected to the positive pole of on the back of the dielectric substrate, and the side length of the square copper plate is 2 mm. The via hole at the other end of the radiation patch is

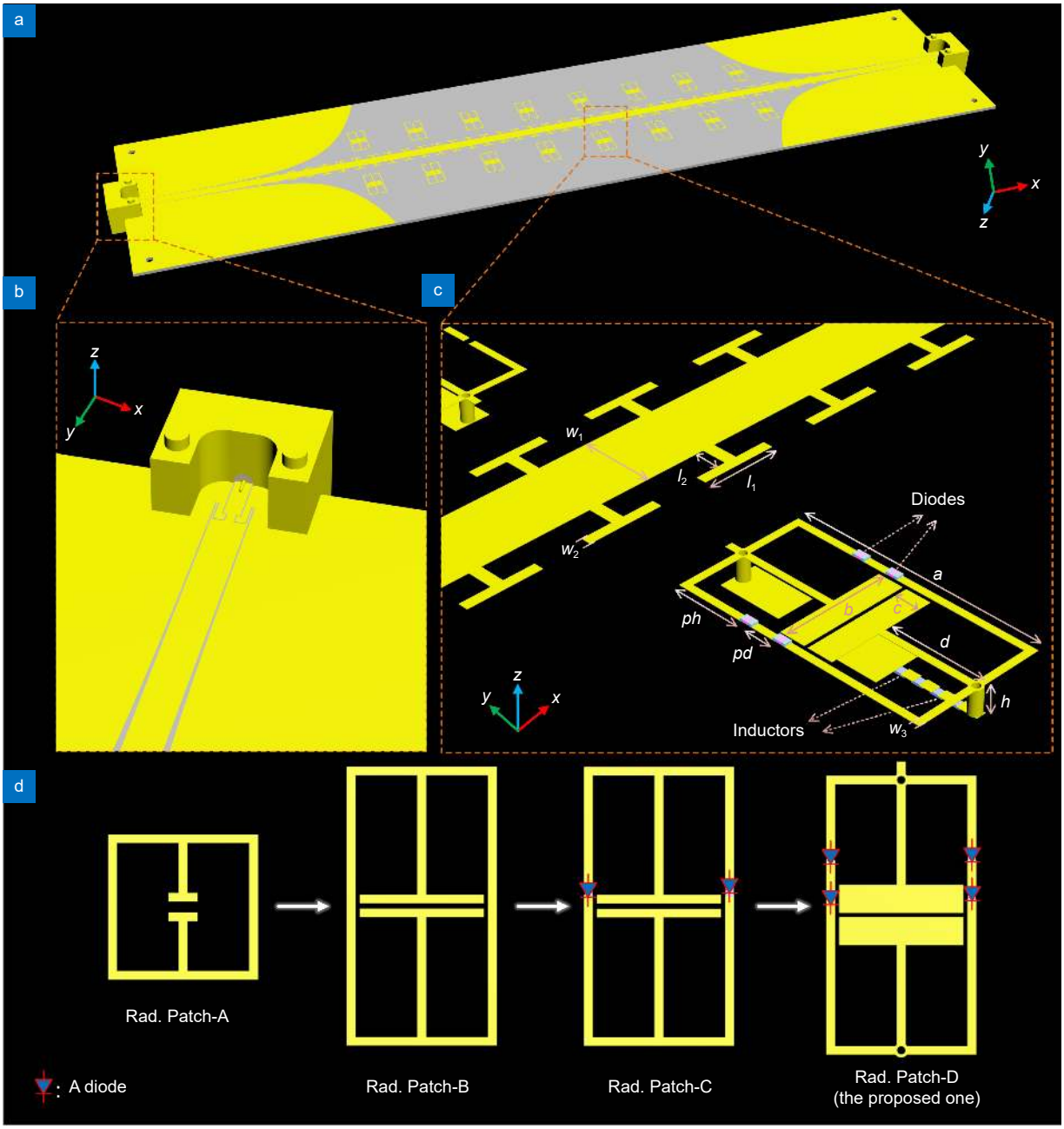

Fig. 4 | (**a**) Schematic of the proposed reconfigurable SSPP-LWA. (**b**) Transition structure diagram for connecting welding free fixtures. (**c**) Enlarged view of unit cells, where the period l_1 = 3.05 mm, l_2 = 1.04 mm, a = 10.0 mm, b = 4.3 mm, c = 1.0 mm, d = 3.925 mm, h = 0.762 mm, pd = 1.1 mm, ph = 2.85 mm, w_1 = 3.0 mm, w_2 = 0.4 mm, and w_3 = 0.3 mm. (**d**) Evolution process of the proposed radiation patch.

connected to the ground. Four 1nH inductors are placed at the ground terminal, with a distance of 0.5 mm between each inductor, and finally connected to a 2.55 mm × 1.5 mm copper sheet for feeding.

The switching of the working state of the antenna is controlled by the bias voltage of the PIN diode. When the PIN diode is turned on, the antenna is in the radiating state; and when it is turned off, the antenna is in the transmission (non-radiating) state. In the topology design of the PIN diode of the patch, the isolation of switching states and the working bandwidth should be weighed. Series switches have the advantage of low transmission loss in broadband but at the price of low isolation. Parallel switches are usually used in combination with quarter-wavelength TLs, which are narrow in nature, but have higher isolation than series switches. In addition, using two or more PIN diodes in series mode can improve the isolation of one PIN diode, and the

same bias current can be used in series connection to save power. In this work, in order to realize broadband performance, high isolation and low-power dissipation, two PIN diodes are designed in series. (Please see Supplementary information Section 4 for the equivalent circuit of the PIN diode used).

Toggle of transmission and radiation

The reconfigurable SSPP-LWA redistributes the current distribution on the antenna by switching the diode between "ON" and "OFF" states, and so as to control the coupling state between the radiation units and the SSPPs TL. The antenna adopts the SSPP TL based on "T"-shaped unit structure as the feed, uses periodically loads radiation units on both sides of the TL to stimulate the higher harmonic for radiation, and selects the −1 order harmonic for single mode radiation. The less-lossy dielectric substrate of the antenna is Taconic TLY-5 (ε_r = 2.2, tanδ = 0.0009) with a thickness of 0.762 mm, and the copper thickness is 0.018mm. The overall size of the designed SSPP-LWA is 269×63.24 mm^2.

The commercial software, Computer Simulation Technology (CST) Microwave Studio was used to conduct time-domain full-wave simulation of the above antenna. Figure 5(a) plots the simulated reflection coefficient (S11) and transmission coefficient (S21). The impedance matching performance of the proposed SSPP-LWA is measured by the Agilent vector network analyzer (VNA) in Fig. 5(b). It can be seen that when the PIN diode is interrupted (OFF of PIN diodes), S11 is low and S21 is high from 8.5 GHz to 13 GHz, and the "transmission" state is realized. In contrast, when the PIN diode is switched ON, the simulated and measured S21 decreased in 9–13 GHz and S11 remains below −10 dB. This result is due to the fact that in this case most energy is successfully coupled to patches and radiated to free space, and the radiation units and the SSPPs TL as a whole work in the "radiation" state. The observed return loss and insertion loss are quite low, indicating a good matching and a good radiation efficiency. To be noted, there is an error between the test result and the simulation result, which is related to the loss of dielectric and active devices, and the insertion loss of cables and SMA connectors in the high-frequency test environment.

To verify the proposed model, we plot the simulated local current distribution of the coupling part and radiation unit in Fig. 5(c, d). When the radiation unit is placed near the TL of SSPPs, there is a current distribution on each radiation unit due to EM coupling. When the PIN diode is switched on, the radiation unit corresponds to the position where the magnetic field of the TL is strong, and the current distribution on the radiation unit forms a closed loop with the corresponding part of the TL, forming a magnetic coupling, as shown in Fig. 5(c). At this time, the current distribution of the overall structure of the radiation unit is along the *Y*-axis, indicating that the radiation unit is equivalent to an electric dipole and radiates EM waves to the free space. On the other hand, when the PIN diode is disconnected, the current distribution of the radiation unit and its corresponding part of the TL does not flow in one direction as a whole, but presents two closed-loop flows in opposite directions, which is equivalent to two magnetic dipoles whose energy cancels each other out. At the same time, there will be four effective pores on the radiation unit. The current distribution is mainly concentrated in the two effective pores below and their current distribution direction is opposite, which is equivalent to the magnetic dipole in the opposite direction, and the coupled electromagnetic energy basically cancels each other, as shown in Fig. 5(d).

There are also some similar studies on the principles of switching or modulating radiation and transmission of waves. Firstly, metasurfaces can convert spatially incident CP beams into spoof surface plasmons (SSP) with the same wave vector through phase gradients in the THz regime[58]. Regarding LWAs, a millimeter-wave beam steerable slot array antenna using an Inter-Digitated Capacitor (IDC) based corrugated substrate integrated waveguide (CSIW) acts as a normal waveguide when the pin diodes are unbiased, but when a segment's pin diodes of IDC-CSIW are activated, it tends to divert the field toward inductive fingers and away from its adjacent longitudinal slot, which then reduces the power radiated from that slot, hence achieving beam reconfigurability[59]. Other modulation types also include adjusting the period length of the antenna by toggling the operation states of the patches between "ON" and "OFF" via pin diodes biasing to achieve the beam-scanning antenna[60–62].

In view of this, when the PIN diode is disconnected, the EM energy in the radiation unit does not radiate out, and most of the energy is transmitted, that is, the antenna changes from the state of leakage wave radiation to the state of transmission. In Fig. 5(e–l), the distributions of simulated and measured near electric field test results

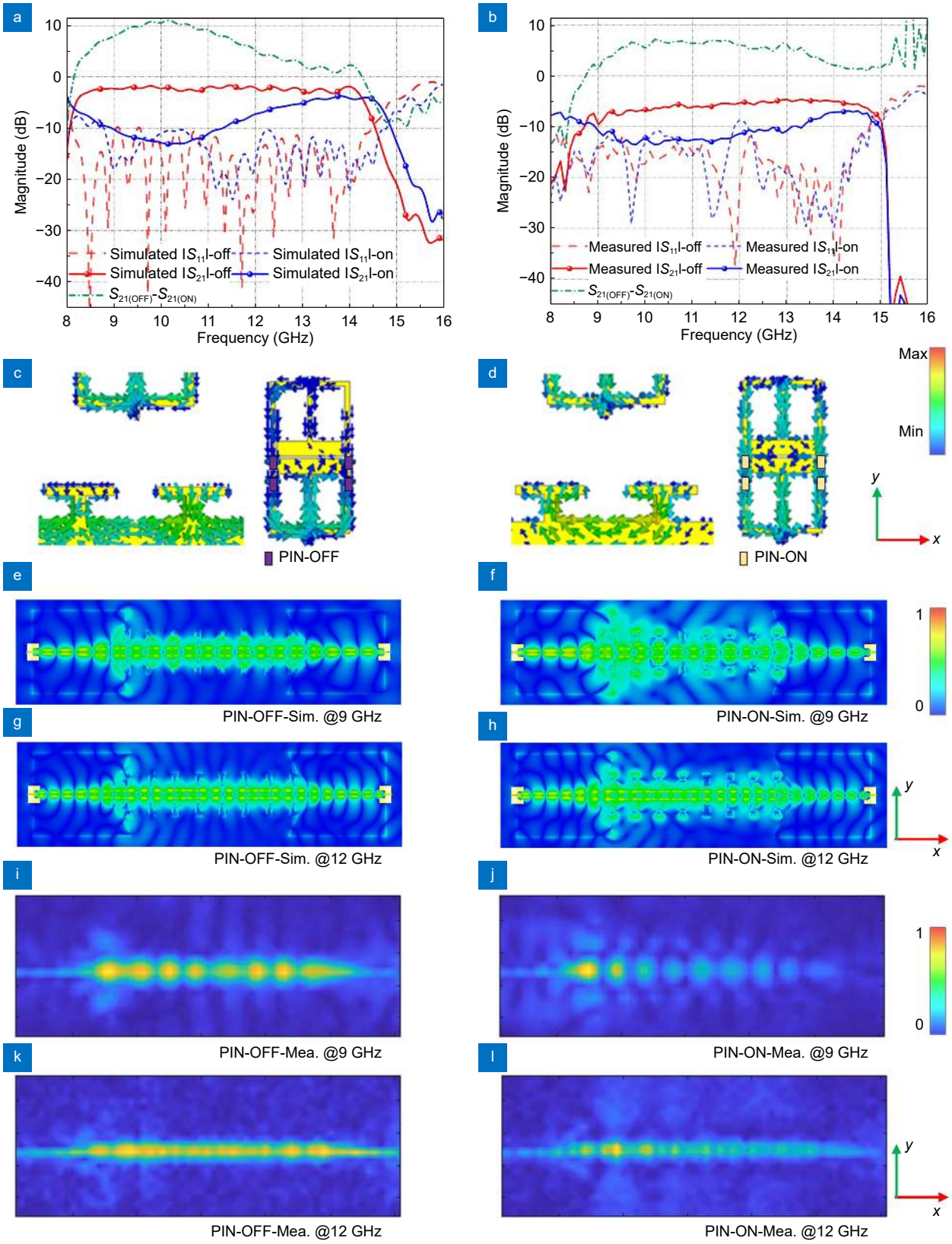

Fig. 5 | Performance of the reconfigurable SSPP-LWA. (**a**) Simulated and (**b**) measured S-parameter of the reconfigurable SSPP-LWA at different working states. The local current distributions of the antenna in two working states, the coupling part and radiation unit during (**c**) radiation state and (**d**) non-radiation state at 11 GHz. When the diode is "ON" or "OFF", the (**e**–**h**) simulated and (**i**–**l**) measured field distributions of the integral structure in the radiating state and the non-radiating state at 9 GHz and 12 GHz.

are plotted. It is worth emphasizing that because of the constraints imposed by the actual test conditions, the phase of the output signal received by the VNA cannot be calibrated based on the input signal generator during the scanning process, resulting in only amplitude values of the electric field being measured. Here, we combine simulated results with the measured ones to present the reconfigurable SSPP-LWA field distribution in the radiation and the non-radiation states. It can be observed that when the field is distributed in a radiating state at 9 GHz and 12 GHz, the energy gradually decreases along the waveguide of the reconfigurable SSPP-LWA. In contrast, in the non-radiating state, the field distribution is clearly transmitted along the TL, which intuitively demonstrates the field variation in the two states. For field distribution at frequencies other than those mentioned above, please see Supplementary information Section 5 for details. In the design, the loss from active components (the diode) are quite noticeable, followed by substrate loss, connectors, and test environment. The designed sample reflects the scenario after accounting for most influencing factors. Our future goal is to further refine the design so as to achieve a lower total loss.

Radiation demonstration of the reconfigurable SSPP-LWA

For more visualized perception of the beam scanning capability, Fig. 6(a–c) shows the simulated 3D radiation patterns in different beam scanning angles. When the frequency increases, the beam scans towards different angles, and a backward to forward beam scanning can be achieved. The amplitudes of electric fields at different frequencies of the structure are also simulated by CST Microwave Studio. It can be clearly observed from Fig. 6(a–c) that, whether it is the three-dimensional far-field pattern or the amplitudes of electric fields at different frequencies of the antenna, it can be seen that as the frequency increases, the beam is directed at different angles, and backward to forward beam scanning can be achieved. At the same time, from near-field simulation results, it can be seen that the amplitude of the EM wave transmitted along the SSPP TL is significantly lower, indicating the leakage of energy.

To gain a more vivid understanding of the beam scanning capability, simulated results for the frequency scanning of reconfigurable SSPP-LWA with two working states are shown in Fig. 6(d, e). The polar plot shows that the beam scans from −43° (at 8.5 GHz) to 5° (at 13 GHz) in the relative central coordinate system. Fig. 6(f) shows that the realized gain of the reconfigurable SSPP-LWA remains in the range of 11.2–7.293 dBi throughout the working frequency band of 8.5 GHz to 13 GHz. The average gain in the radiated state is 7.3 dBi higher than that in the non-radiated state. Through the comparison of the total radiated power in the two states of reconfigurable SSPP-LWA, we can also see that the two states have excellent switching effect in Fig. 6(g).

To verify the above theoretical analysis and demonstrate the good performance, the prototype of the proposed SSPP-LWA is fabricated and measured. The radiation patterns are tested in an anechoic chamber environment, as shown in Fig. 7(a). The front and back enlarged photos of the prototype are shown in Fig. 7(b, c). Figure 7(d–g) shows the measured radiation patterns of the proposed beam-scanning antenna from 8.5 to 13 GHz with co-polarization and cross-polarization under two working states. The measured beam angle scans from −44° to 4.7°, whereas the measured gain ranges from 8.36 to 4.4 dBi. It can be seen that the beam steers from backward to forward with scanning ranges of −44° at 8.5 GHz, 34° at 9 GHz, −12° at 11 GHz, and 4.7° at 13 GHz, respectively. The measured results are given as a validation of the design. These gain drops are mainly caused by the error of the fabrication and measurement system, especially, the coaxial feeder and active device loss and radiation effects from the turntable base lead to amplitude drop. The gain curves of the co-polarization and cross-polarization measurements are given in Fig. 7(h, i). The radiation gain is lower when the diode is OFF (transmission state), and in the case of cross polarization. The average gain of the ON and OFF operating states is 6.9 dBi and 1.18 dBi, respectively. And the gain of each frequency point can be read in the Fig. 7(h). The radiation pattern results and gain curves of two states also show that the designed SSPP-LWA has good state switching and frequency beam scanning characteristics.

Perceptible platform based on reconfigurable SSPP-LWA and computer vision

In wireless communication, radar system can detect and track targets in the complex EM environment. However, due to the high cost, large size and complex design, other technologies are urgently needed to make up for it. Fortunately, with the fast development of computer vision technology, intuitive, reliable, and cost-effective target detection and tracking become possible in many

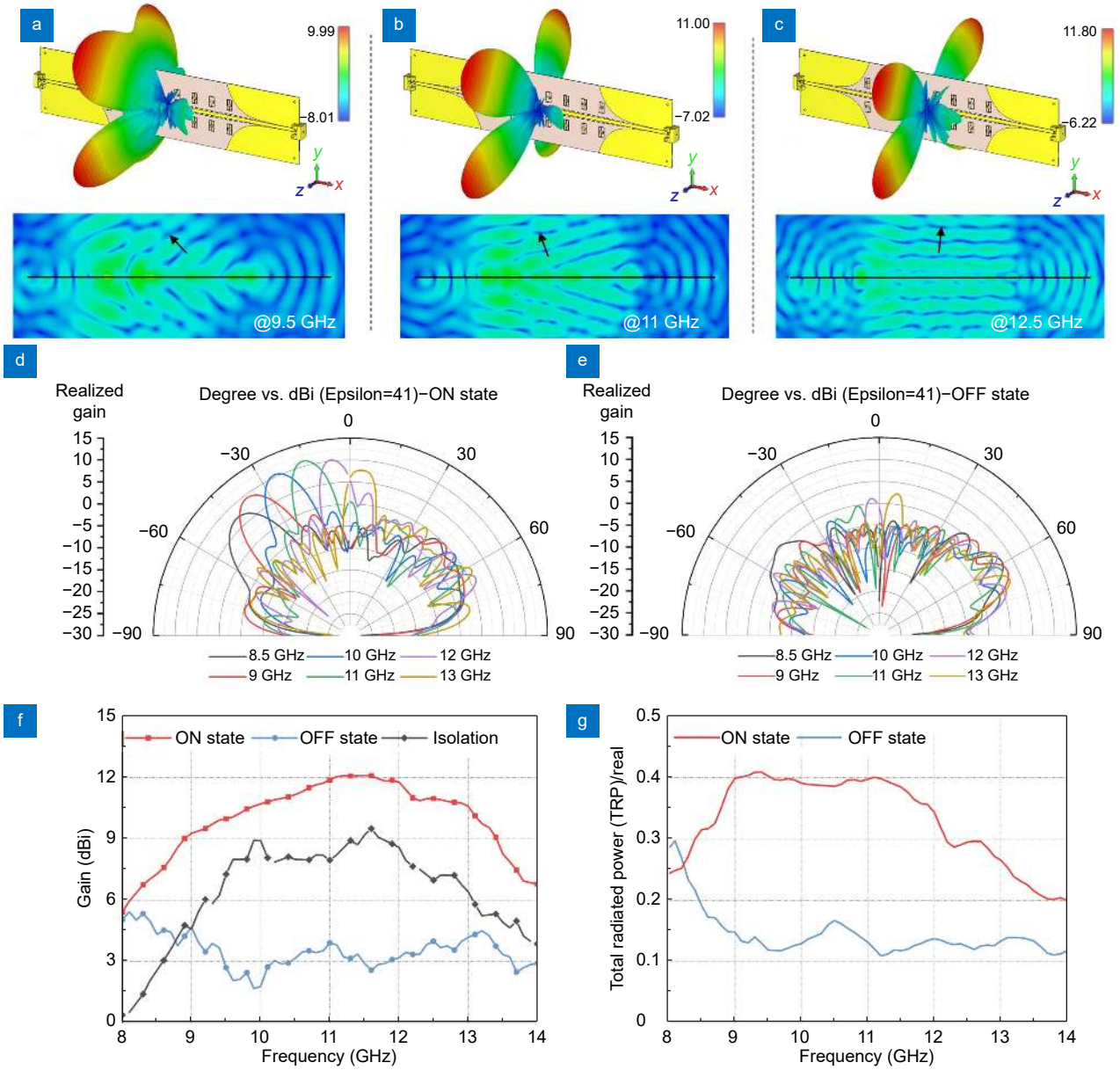

Fig. 6 | Simulated 3D radiation patterns and amplitude distributions of electric fields at different beam scanning angles for the reconfigurable SSPP-LWA. (**a**) 9.5 GHz. (**b**) 11 GHz. (**c**) 12.5 GHz. Simulated far-field radiation patterns of the proposed SSPP-LWA of (**d**) radiation and (**e**) transmission states at different frequencies. (**f**) Gains and (**g**) radiation power of the proposed reconfigurable SSPP-LWA.

application scenarios. Moreover, AI-enabled computer vision (CV) technology is evolving rapidly, which can solve more complicated problems and serve as an aid to intelligent communications. Here, it is designed as a perceptible innovative technology, with the proposed smart SSPP-LWA system to realize an intelligent perceptible platform that combines perception and communication.

Target detection based radiation switchable SSPP-LWA

The externally perceptive platform is shown in Fig. 8(a), which consists of an Intel RealSense Depth Camera D435i (RS-Camera), control system (a computer) and Field-Programmable Gate Array (FPGA). First, the images of the toy car are taken by a RS-Camera located on the reconfigurable SSPP-LWA at the rate of 40 FPS (frames per second), and each image is selected by the convolutional neural network (CNN) based on YOLOv4-tiny. Here, we use the toy car to represent the detection target of the scene. The RS-Camera collects moving targets, and the control system connects with the camera, feeds back the position of the target, and then transmits

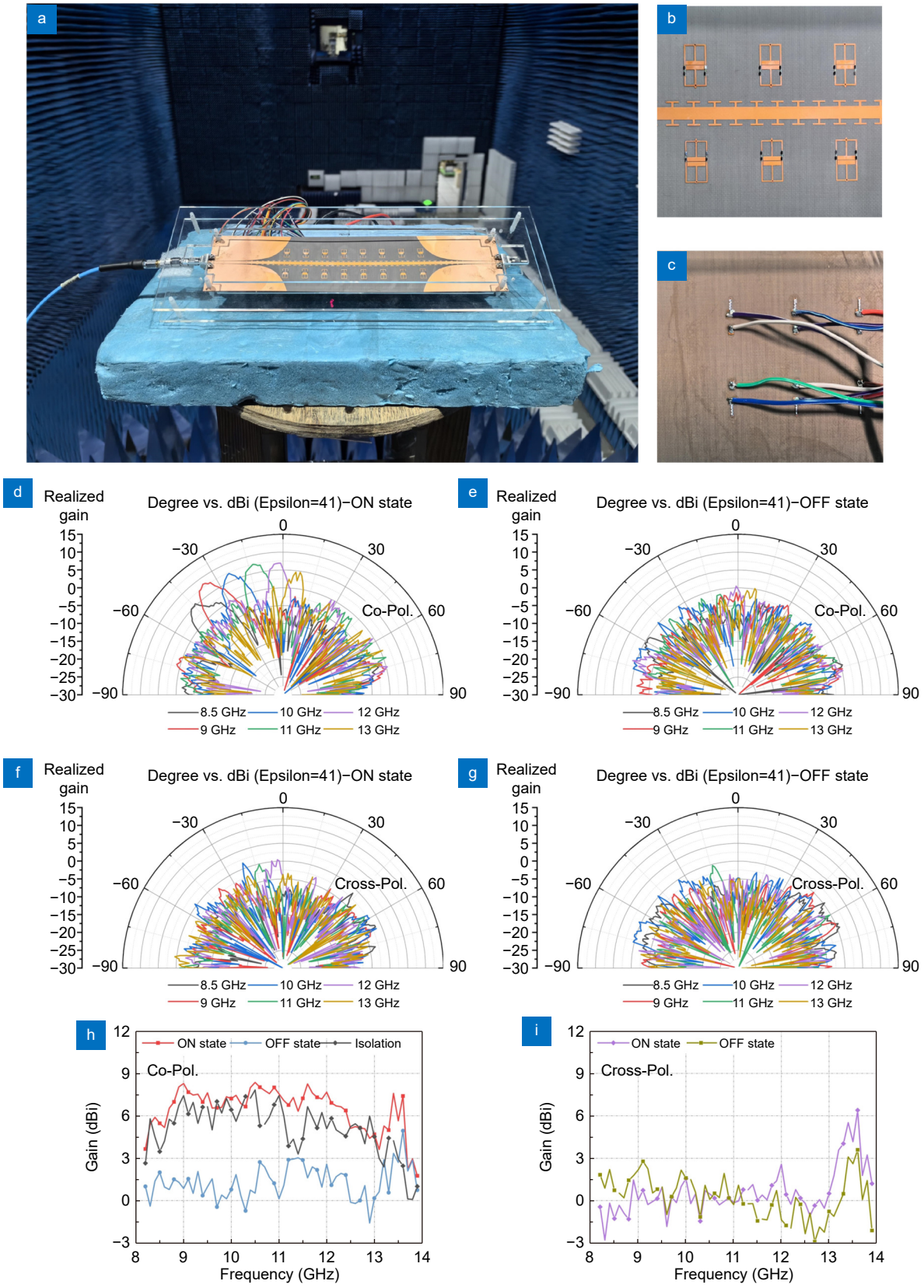

Fig. 7 | (**a**) Prototype of the reconfigurable SSPP-LWA in a microwave anechoic chamber. Enlarged part of the (**b**) front and (**c**) back of the antenna. Measured radiation pattern of (**d**) radiation and (**e**) transmission states with co-polarization. Measured radiation pattern of (**f**) radiation and (**g**) transmission states with cross-polarization. Measured gain with (**h**) co-polarization and (**i**) cross-polarization.

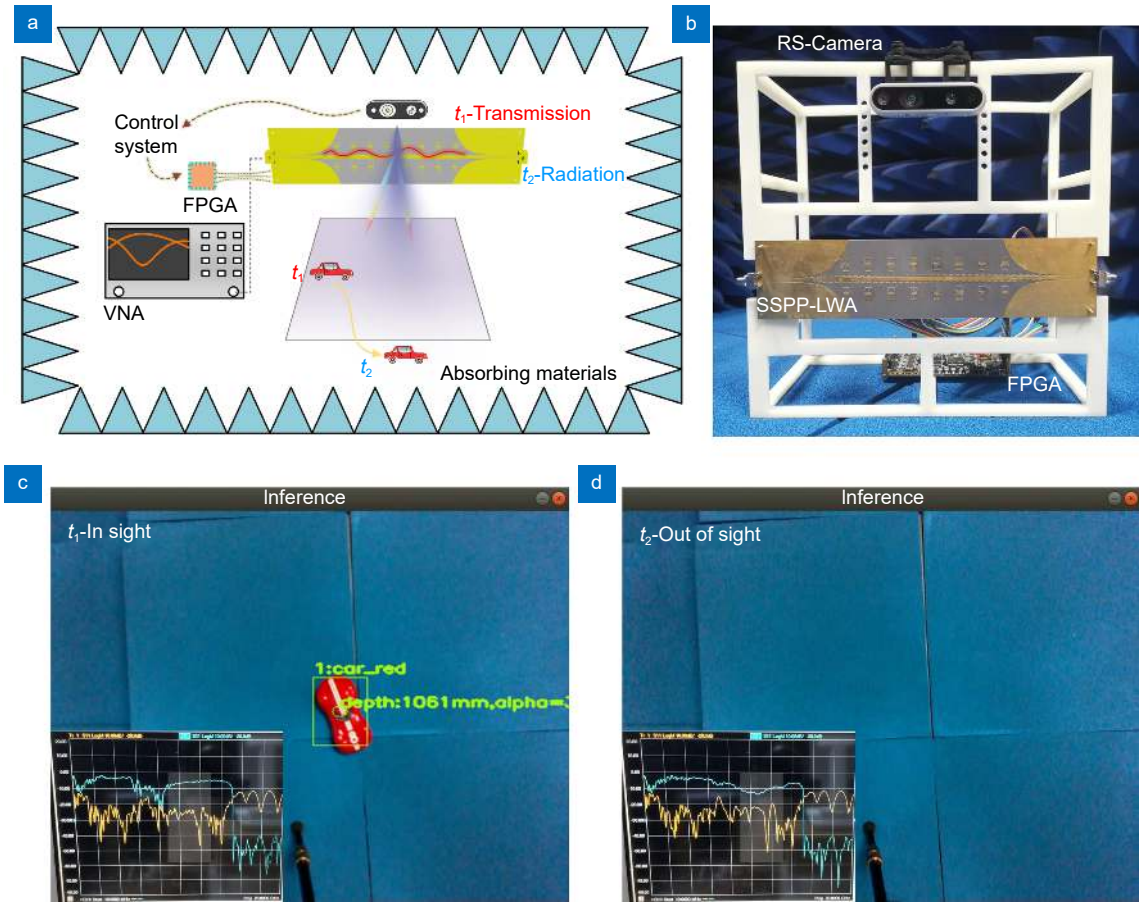

Fig. 8 | The position of the moving car is processed in the control system, and all bias voltages are instantly calculated and supplied to the smart SSPP-LWA. The working state is tested by a VNA. (**a**) Test scenarios, please see Supporting Information 6 for details. (**b**) A picture of the externally perceivable SSPP-LWA system. The results of two test scenarios in which the target (**c**) appears or (**d**) disappears.

the corresponding voltage sequence to the FPGA.

In the test scene, we use a toy car instead of a detector or jammer as the target, and the field of view in Fig. 8(a) that can be captured by the camera is the area where the target is moving, the field of view is the range of angles the camera can see, including depth information. When we move the car into or out of the target area, the antenna can quickly change the non-radiation/radiation state accordingly. In addition, the smart SSPP-LWA is connected to Agilent Vector Network Analyzer N5230C (VNA), and the state of the smart SSPP-LWA can be observed through the S-parameter in VNA. The process of the car appearing and disappearing from the field of view is shown in Fig. 8(c, d). The lower right corner of each figure is the S-parameter curve shown in VNA. When the car moves to the blue area that can be captured by the RS-camera, the car will be marked. At this time, the FPGA output level is low, the PIN diode on the smart SSPP-LWA is disconnected and the antenna is in the transmission (non-radiation) state. The FPGA in the system has a 20-channel 3.3 V analog output port, each driving four diodes per radiation patch. Outputs can be switched via a serial port tool, allowing independent power supply for each radiation unit. In far-field testing without active control, a DC power source under 5 V and a current limit of 40 mA can be used as an alternative and can operate stably for a long time. The state of the antenna can be verified through the S-parameter feedback in VNA, which corresponds to the transmission state. When there is no toy car appears in the field of view, the FPGA outputs high level at this time, and the PIN diode on the smart SSPP-LWA is switched on, the antenna is in the radiation state, accompanied by low S11 and S21 in VNA. Please see Supplementary Movie 1 for details. The working states are switched by the SSPP-LWA under the control of the real-time varying coding sequence to keep tracking the target at a sampling speed of 0.2 s (see Supplementary information Section 8 for details). The speed limit lies in the sampling speed of the RS-Camera.

It can be observed that the S-parameter is very consistent with the measured results in Fig. 5(b). Therefore, in the external perceptive platform of this scene, the smart SSPP-LWA realizes automatically control its working state, which can achieve wireless communication security in the airspace to a certain extent.

Beam tracking of the SSPP-LWA with vision aid

We have carried out the intelligent system experiment of beam tracking. By detecting the location of the receiver (a horn antenna) with a RS-Camera, we can send the frequency instruction of the corresponding beam direction to the signal generator (the SSPP LWA), so as to realize the closed-loop operation of the system without human instruction. The system consists of a signal generator (SA, Keysight E8257D), a signal analyzer (SG), the SSPP-LWA, a RS-Camera, a computer and a receiver (a dual-ridged horn antenna, 750 MHz to 18 GHz). The SG is connected to the LWA, the receiver is connected to the SA, and the computer controls the RS-Camera and SG respectively, as shown in Fig. 9(a, b). In order to more accurately show the power acceptance of the SSPP-LWA at a certain distance, we have carried out the near-field test of the SSPP-LWA, please see Supplementary information Section 7 for details.

Firstly, we tested the accepted energy values for all frequencies without the camera working. It can be seen that the receiving antenna is fixed on a slide rail and bisects ten moving points in a horizontal movement of 1.5 m. Each point position measures the received energy at different emission frequencies. The signal generator transmits 9–13 GHz EM waves and records them every 0.2 GHz. The task of the vision-aided SSPP-LWA is to accurately radiate the EM waves to the horn antenna at the

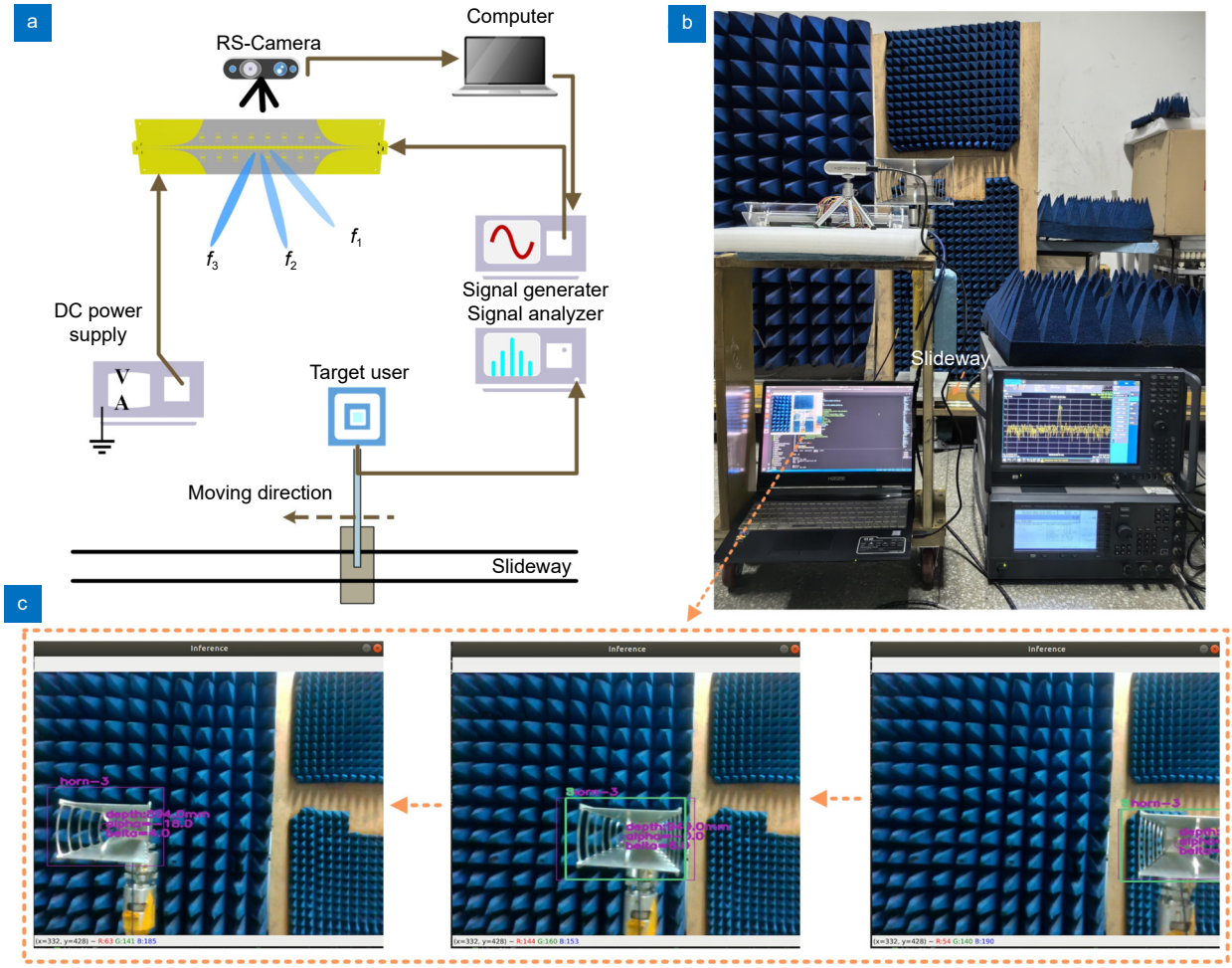

Fig. 9 | (**a**) Test scenarios of beam tracking, in which a broadband horn antenna moves on the slide rail as the target user, and the RS-Camera captures the position information of the target user, as shown below. It then feeds back to the computer and sends frequency instructions to the signal generator. (**b**) Detailed connection process of the experimental device. (**c**) Experimental results of picture frames at three different positions of the target user on the moving path.

receiver side based on the visual information. In test progress, as for the vision-based beam tracking scheme, we use object detection and CV technology to obtain the position information of the horn antennas with respect to the SSPP-LWA. Then beam tracking is implemented in two stages. In the first stage, since we have actually tested the radiation status of SSPP-LWA, we can determine the correspondence of the angle with regard to the frequency. In the second stage, according to the coordinates of the target user, SSPP-LWA can obtain the desired beam direction and select the corresponding codeword in the precoder to achieve beam tracking. We can get the direction of the predicted bounding box of the target user at a certain moment through the visual algorithm, as shown in Fig. 9(a).

During testing, we move the target user within coverage areas that include SSPP-LWA beamforming. To highlight the effectiveness of vision, we plot in one diagram with visual aids and in all situations. When there is no visual aid, the traditional frequency scanning method, in which the feedback procedure is ignored, traverses the received power at each frequency point at all locations. When there is visual assistance, the strategy of beam tracking is: first use RS-Camera to feedback the position of the target user in the field of view, and when the user is outside the beam scanning range, the computer does not send instructions to the SG. And when the user is within the coverage range of SSPP-LWA beamforming, the computer sends the frequency instruction of the response to SG according to the returned angle information. The SSPP-LWA's operating frequency is adjusted from 8.5 GHz to 13.1 GHz to allow the platform to operate at a sufficient scanning range. It can be seen that the blue five-star mark records the receiving power value of different positions in Fig. 10, and through the change of frequency, it is very stable to maintain a high receiving power, ensuring the high quality of communication. The range of the test is beyond the beam-scanning area, but SSPP-LWA still retains the scattered beam with low gain in the region of more than 5° (Moving more than 100 cm), where SSPP-LWA still executes the command, but the sensitivity decreases due to the decreased gain value.

At the same time, there is no additional feedback process and beam training overhead throughout the communication. For traditional passive devices, it is basically difficult to achieve beam tracking and dynamic switching. The smart system adjusts the operating frequency according to the information of target detection in the process of beam scanning to avoid spectrum conflict, improve spectrum utilization, and reduce overhead.

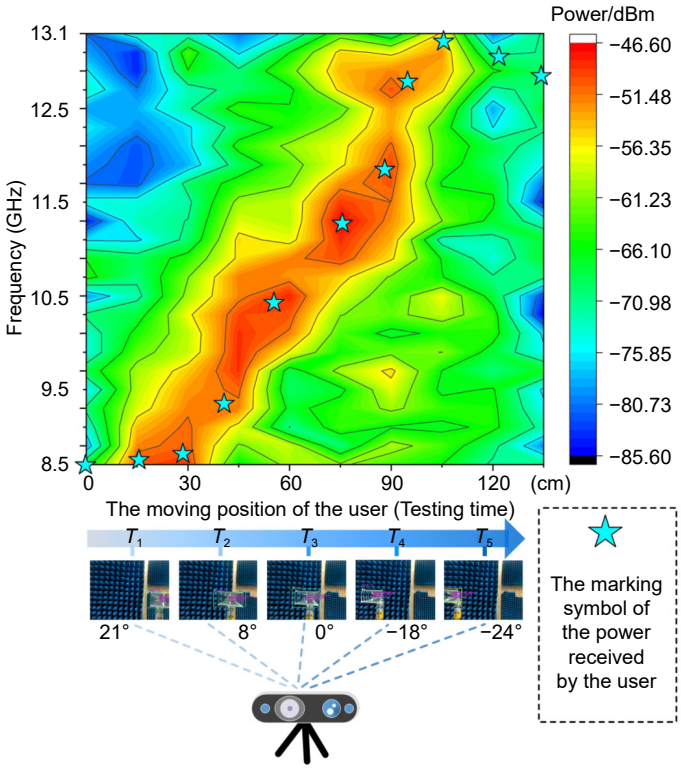

Fig. 10 | The received power of the target user corresponds to different frequencies during the movement. The blue pentagon is marked as the received power of the target user with vision aid.

Conclusions

In this paper, we propose a smart SSPP-LWA with external perceptibility, which can realize the adaptive real-time switching between the radiation state and the non-radiation state and beam tracking by regulating the coupling unit. In two intelligent communication scenarios, the SSPP-LWA obtains the real-time location information of the external jammer or target user through the CV, switches the working states accordingly, and realizes automatic tracking of moving target by adjusting the input frequency. Leveraging the capabilities of beam reconfiguration and external perception, the proposed SSPP-LWA serves as a prime contender for smart systems, offering the ability to autonomously select optimal operating modes and intelligent communication in dynamic, complex environments.

References

1. Barnes WL, Dereux A, Ebbesen TW. Surface plasmon subwavelength optics. *Nature* **424**, 824–830 (2003).
2. Garcia-Vidal FJ, Martín-Moreno L, Pendry JB. Surfaces with

holes in them: new plasmonic metamaterials. *J Opt A Pure Appl Opt* **7**, S97–S101 (2005).
3. Gan QQ, Fu Z, Ding YJ et al. Ultrawide-bandwidth slow-light system based on THz plasmonic graded metallic grating structures. *Phys Rev Lett* **100**, 256803 (2008).
4. Shen XP, Cui TJ, Martin-Cano D et al. Conformal surface plasmons propagating on ultrathin and flexible films. *Proc Natl Acad Sci USA* **110**, 40–45 (2013).
5. Ma HF, Shen XP, Cheng Q et al. Broadband and high-efficiency conversion from guided waves to spoof surface plasmon polaritons. *Laser Photon Rev* **8**, 146–151 (2014).
6. Kianinejad A, Chen ZN, Qiu CW. Low-loss spoof surface plasmon slow-wave transmission lines with compact transition and high isolation. *IEEE Trans Microw Theory Tech* **64**, 3078–3086 (2016).
7. He PH, Zhang HC, Gao XX et al. A novel spoof surface plasmon polariton structure to reach ultra-strong field confinements. *Opto-Electron Adv* **2**, 190001 (2019).
8. Wang M, Sun S, Ma HF et al. Supercompact and ultrawideband surface plasmonic bandpass filter. *IEEE Trans Microw Theory Tech* **68**, 732–740 (2020).
9. Ye LF, Chen Y, Wang ZY et al. Compact spoof surface plasmon polariton waveguides and notch filters based on meander-strip units. *IEEE Photonics Technol Lett* **33**, 135–138 (2021).
10. Liu YQ, Xu KD, Li JX et al. Millimeter-wave E-plane waveguide bandpass filters based on spoof surface plasmon polaritons. *IEEE Trans Microw Theory Tech* **70**, 4399–4409 (2022).
11. Liu XY, Lei Y, Zheng X et al. Reconfigurable spoof plasmonic coupler for dynamic switching between forward and backward propagations. *Adv Mater Technol* **7**, 2200129 (2022).
12. Niu LY, He PH, Fan Y et al. Gain‐associated nonlinear phenomenon in single‐conductor odd‐mode plasmonic metamaterials. *Laser Photon Rev* **16**, 2100619 (2022).
13. Gao XX, Zhang JJ, Luo Y et al. Reconfigurable parametric amplifications of spoof surface plasmons. *Adv Sci* **8**, 2100795 (2021).
14. Liu LL, Wu L, Zhang JJ et al. Backward phase matching for second harmonic generation in negative-index conformal surface plasmonic metamaterials. *Adv Sci* **5**, 1800661 (2018).
15. Zhang J, Zhang HC, Gao XX et al. Integrated spoof plasmonic circuits. *Sci Bull* **64**, 843–855 (2019).
16. Zhang HC, Zhang LP, He PH et al. A plasmonic route for the integrated wireless communication of subdiffraction-limited signals. *Light Sci Appl* **9**, 113 (2020).
17. Tang WX, Zhang HC, Ma HF et al. Concept, theory, design, and applications of spoof surface plasmon polaritons at microwave frequencies. *Adv Opt Mater* **7**, 1800421 (2019).
18. Pu MB, Ma XL, Guo YH et al. Theory of microscopic meta-surface waves based on catenary optical fields and dispersion. *Opt Express* **26**, 19555–19562 (2018).
19. Guo YH, Zhang ZJ, Pu MB et al. Spoof plasmonic metasurfaces with catenary dispersion for two-dimensional wide-angle focusing and imaging. *iScience* **21**, 145–156 (2019).
20. Luo XG, Pu MB, Guo YH et al. Catenary functions meet electromagnetic waves: opportunities and promises. *Adv Opt Mater* **8**, 2001194 (2020).
21. Gomez-Tornero JL, Quesada-Pereira FD, Alvarez-Melcon A. Analysis and design of periodic leaky-wave antennas for the millimeter waveband in hybrid waveguide-planar technology. *IEEE Trans Antennas Propag* **53**, 2834–2842 (2005).
22. Jackson DR, Caloz C, Itoh T. Leaky-wave antennas. *Proc IEEE* **100**, 2194–2206 (2012).
23. Wang M, Ma HF, Tang WX et al. A dual-band electronic-scanning leaky-wave antenna based on a corrugated microstrip line. *IEEE Trans Antennas Propag* **67**, 3433–3438 (2019).
24. Cameron TR, Eleftheriades GV. Experimental validation of a wideband metasurface for wide-angle scanning leaky-wave antennas. *IEEE Trans Antennas Propag* **65**, 5245–5256 (2017).
25. Mackay AJ, Eleftheriades GV. Meandered and dispersion-enhanced planar leaky-wave antenna with fast beam scanning. *IEEE Antennas Wirel Propag Lett* **20**, 1596–1600 (2021).
26. Karmokar DK, Esselle KP, Bird TS. Wideband microstrip leaky-wave antennas with two symmetrical side beams for simultaneous dual-beam scanning. *IEEE Trans Antennas Propag* **64**, 1262–1269 (2016).
27. Chen HY, Ma H, Li YF et al. Wideband frequency scanning spoof surface plasmon polariton planar antenna based on transmissive phase gradient metasurface. *IEEE Antennas Wirel Propag Lett* **17**, 463–467 (2018).
28. Wang J, Zhao L, Hao ZC et al. Wide-angle frequency beam scanning antenna based on the higher-order modes of spoof surface plasmon polariton. *IEEE Trans Antennas Propag* **68**, 7652–7657 (2020).
29. Ge SK, Zhang QF, Rashid AK et al. Analysis of asymmetrically corrugated goubau-line antenna for endfire radiation. *IEEE Trans Antennas Propag* **67**, 7133–7138 (2019).
30. Zu HR, Wu B, Zhao YT et al. Dual-band antenna with large beam steering angle incorporating endfire and frequency scanning modes using double-layer SSPPs structure. *IEEE Trans Antennas Propag* **70**, 46–55 (2022).
31. Sarkar A, Lim S. Annular surface plasmon polariton-based frequency-scanning leaky-wave antenna for full azimuth coverage. *IEEE Trans Antennas Propag* **70**, 180–188 (2022).
32. Yin JY, Ren J, Zhang Q et al. Frequency-controlled broad-angle beam scanning of patch array fed by spoof surface plasmon polaritons. *IEEE Trans Antennas Propag* **64**, 5181–5189 (2016).
33. Zhang G, Zhang QF, Chen YF et al. High-scanning-rate and wide-angle leaky-wave antennas based on glide-symmetry goubau line. *IEEE Trans Antennas Propag* **68**, 2531–2540 (2020).
34. Lau JY, Hum SV. Reconfigurable transmitarray design approaches for beamforming applications. *IEEE Trans Antennas Propag* **60**, 5679–5689 (2012).
35. Hong W, Jiang ZH, Yu C et al. Multibeam antenna technologies for 5G wireless communications. *IEEE Trans Antennas Propag* **65**, 6231–6249 (2017).
36. Ahmed I, Khammari H, Shahid A et al. A survey on hybrid beamforming techniques in 5G: architecture and system model perspectives. *IEEE Commun Surv Tutorials* **20**, 3060–3097 (2018).
37. Zhao DX, Gu P, Zhong JC et al. Millimeter-wave integrated phased arrays. *IEEE Trans Circuits Syst I Regul Pap* **68**, 3977–3990 (2021).
38. Rappaport TS, Gutierrez F, Ben-Dor E et al. Broadband millimeter-wave propagation measurements and models using adaptive-beam antennas for outdoor urban cellular communications. *IEEE Trans Antennas Propag* **61**, 1850–1859 (2013).
39. Huang LB, Li X, Wan WT et al. Adaptive FDA radar transmit power allocation for target detection enhancement in clutter environment. *IEEE Trans Veh Technol* **72**, 11111–11121 (2023).

40. Wang HL, Ma HF, Chen M et al. A reconfigurable multifunctional metasurface for full‐space control of electromagnetic waves. *Adv Funct Mater* **31**, 2100275 (2021).
41. Wang J, Kühne J, Karamanos T et al. All‐dielectric crescent metasurface sensor driven by bound states in the continuum. *Adv Funct Mater* **31**, 2104652 (2021).
42. Wu XY, Feng HY, Wan F et al. An Ultrathin, Fast-Response, Large-Scale Liquid-Crystal-Facilitated Multi-Functional Reconfigurable Metasurface for Comprehensive Wavefront Modulation. *Adv Mater* **36**, 2402170 (2024).
43. Liu TH, Li WH, Meng YY et al. Six‐mode orbital angular momentum generator enabled by helicity‐assisted full‐space metasurface with flexible manipulation of phase, polarization, and spatial information. *Adv Opt Mater* **10**, 2102638 (2022).
44. Di Renzo M, Zappone A, Debbah M et al. Smart radio environments empowered by reconfigurable intelligent surfaces: how it works, state of research, and the road ahead. *IEEE J Sel Areas Commun* **38**, 2450–2525 (2020).
45. Wu QQ, Zhang R. Intelligent reflecting surface enhanced wireless network via joint active and passive beamforming. *IEEE Trans Wirel Commun* **18**, 5394–5409 (2019).
46. Cui TJ, Qi MQ, Wan X et al. Coding metamaterials, digital metamaterials and programmable metamaterials. *Light Sci Appl* **3**, e218 (2014).
47. Zhu RC, Wang JF, Qiu TS et al. Direct field-to-pattern monolithic design of holographic metasurface via residual encoder-decoder convolutional neural network. *Opto-Electron Adv* **6**, 220148 (2023).
48. Qian C, Zheng B, Shen YC et al. Deep-learning-enabled self-adaptive microwave cloak without human intervention. *Nat Photonics* **14**, 383–390 (2020).
49. Ma Q, Bai GD, Jing HB et al. Smart metasurface with self-adaptively reprogrammable functions. *Light Sci Appl* **8**, 98 (2019).
50. Luo ZJ, Ren XY, Zhou L et al. A high‐performance nonlinear metasurface for spatial‐wave absorption. *Adv Funct Mater* **32**, 2109544 (2022).
51. Wan X, Wang JW, Huang ZA et al. Space–time–frequency modulation mechanisms of monochromatic and nonmonochromatic electromagnetic waves on a digital programmable transmission metasurface. *Adv Funct Mater* **32**, 2107557 (2022).
52. Ouyang M, Gao FF, Wang YC et al. Computer vision-aided reconfigurable intelligent surface-based beam tracking: prototyping and experimental results. *IEEE Trans Wirel Commun* **22**, 8681–8693 (2023).
53. Li WH, Ma Q, Liu C et al. Intelligent metasurface system for automatic tracking of moving targets and wireless communications based on computer vision. *Nat Commun* **14**, 989 (2023).
54. Wang B, Liu JH, Zhu SJ et al. A dual-input moving object detection method in remote sensing image sequences via temporal semantics. *Remote Sens* **15**, 2230 (2023).
55. Nigam N, Singh DP, Choudhary J. A review of different components of the intelligent traffic management system (ITMS). *Symmetry* **15**, 583 (2023).
56. Sha D, Gao JQ, Yang D et al. Calibrating stochastic traffic simulation models for safety and operational measures based on vehicle conflict distributions obtained from aerial and traffic camera videos. *Accid Anal Prev* **179**, 106878 (2023).
57. Kong GS, Ma HF, Cai BG et al. Continuous leaky-wave scanning using periodically modulated spoof plasmonic waveguide. *Sci Rep* **6**, 29600 (2016).
58. Wang Z, Li SQ, Zhang XQ et al. Excite spoof surface plasmons with tailored wavefronts using high‐efficiency terahertz metasurfaces. *Adv Sci* **7**, 2000982 (2020).
59. Bansal A, Panagamuwa CJ, Whittow WG. Millimeter-wave beam steerable slot array antenna using an inter-digitated capacitor based corrugated SIW. *IEEE Trans Antennas Propag* **70**, 11761–11770 (2022).
60. Wang Z, Dong Y. Amplitude and frequency modulated leaky wave antenna for reconfigurable intelligent radiation. *IEEE Trans Antennas Propag* **72**, 2189–2201 (2024).
61. Yang D, Nam S. Frequency reconfigurable beam scanning squarely modulated reactance surface antenna with period and surface reactance control. *IEEE Access* **11**, 72552–72561 (2023).
62. Wang SZ, Li Z, Wei B et al. A *Ka*-band circularly polarized fixed-frequency beam-scanning leaky-wave antenna based on groove gap waveguide with consistent high gains. *IEEE Trans Antennas Propag* **69**, 1959–1969 (2021).

Acknowledgements

We are grateful for financial supports from the National Natural Science Foundation of China (Grant Nos. 62288101, and 61971134), National Key Research and Development Program of China (Grant Nos. 2021YFB3200502, and 2017YFA0700200), the Major Project of the Natural Science Foundation of Jiangsu Province (Grant No. BK20212002), the Fundamental Research Funds for Central Universities (Grant No. 2242021R41078), and the 111 Project (Grant No. 111-2-05).

Author contributions

W. H. Li, W. X. Tang, and T. J. Cui conceived the idea, conducted the theoretical analysis, and wrote the paper. W. H. Li and J. Chen proposed the concept of leaky-wave antenna and built the proof-of-principle prototype system. W. H. Li, J. Chen, S. Z. Gao, L. Y. Niu, J. X. Wei, R. S. Sun and Y. Q. Wei conducted experiments and data processing. T. J. Cui and W. X. Tang provided suggestions and comments and helped to organize and revise the draft. All authors discussed the results and contributed to the manuscript.

Competing interests

The authors declare no competing financial interests.

Supplementary information

Supplementary information for this paper is available at https://doi.org/10.29026/oea.2024.240040

Scan for Article PDF